

PAPER • OPEN ACCESS

Phase- and intensity-resolved measurements of above threshold ionization by few-cycle pulses

To cite this article: M Kübel *et al* 2018 *J. Phys. B: At. Mol. Opt. Phys.* **51** 134007

View the [article online](#) for updates and enhancements.

You may also like

- [Chirp and carrier-envelope-phase effects in the multiphoton regime: measurements and analytical modeling of strong-field ionization of sodium](#)
D Zille, D Adolph, M Möller et al.
- [Subfemtosecond directional control of chemical processes in molecules](#)
Ali S Alnaser and Igor V Litvinyuk
- [Benchmarking strong-field ionization with atomic hydrogen](#)
D Kielpinski, R T Sang and I V Litvinyuk

Phase- and intensity-resolved measurements of above threshold ionization by few-cycle pulses

M Kübel¹ , M Arbeiter², C Burger^{1,3}, Nora G Kling¹, T Pischke¹, R Moshhammer⁴, T Fennel^{2,5} , M F Kling^{1,3}  and B Bergues^{1,3,6}

¹ Department für Physik, Ludwig-Maximilians-Universität, Am Coulombwall 1, D-85748 Garching, Germany

² Institute of Physics, University of Rostock, Universitätsplatz 3, D-18051 Rostock, Germany

³ Max-Planck-Institut für Quantenoptik, Hans-Kopfermann-Str. 1, D-85748 Garching, Germany

⁴ Max-Planck-Institut für Kernphysik, D-69117 Heidelberg, Germany

⁵ Max-Born-Institut, Max-Born-Straße 2A, D-12489 Berlin, Germany

E-mail: matthias.kuebel@physik.uni-muenchen.de, thomas.fennel@uni-rostock.de and boris.bergues@mpq.mpg.de

Received 24 January 2018, revised 19 April 2018

Accepted for publication 17 May 2018

Published 11 June 2018



CrossMark

Abstract

We investigate the carrier-envelope phase (CEP) and intensity dependence of the longitudinal momentum distribution of photoelectrons resulting from above threshold ionization of argon by few-cycle laser pulses. The intensity of the pulses with a center wavelength of 750 nm is varied in a range between 0.7×10^{14} and 5.5×10^{14} W cm⁻². Our measurements reveal a prominent maximum in the CEP-dependent asymmetry at photoelectron energies of $2 U_p$ (U_p being the ponderomotive potential), that is persistent over the entire intensity range. Further local maxima are observed around 0.3 and $0.8 U_p$. The experimental results are in good agreement with theoretical results obtained by solving the three-dimensional time-dependent Schrödinger equation. We show that for few-cycle pulses, the amplitude of the CEP-dependent asymmetry provides a reliable measure for the peak intensity on target. Moreover, the measured asymmetry amplitude exhibits an intensity-dependent interference structure at low photoelectron energy, which could be used to benchmark model potentials for complex atoms.

Keywords: strong-field physics, above threshold ionization, few-cycle pulses, carrier-envelope phase, laser intensity


(Some figures may appear in colour only in the online journal)

1. Introduction

Above threshold ionization (ATI) of an atomic or molecular target is the absorption of multiple photons in excess of the ionization energy from a short and intense laser pulse

⁶ Author to whom any correspondence should be addressed.

[1–3]. ATI is at the heart of many phenomena involving the interaction of matter with strong laser fields and has led to several applications including high-harmonic generation [4] and attosecond metrology [5, 6]. As such, ATI photoelectron spectra have been attracting a lot of attention over the past four decades, see e.g. [1, 7–14]. They have been utilized to measure physical quantities such as photoionization time delays [15, 16], or molecular orbitals [17] and dynamics [18–21]. Meanwhile, the different characteristic features that ATI spectra exhibit at high [10], medium [22–24], and low [13, 25, 26] energies, have been investigated in numerous studies, and their origin could be

 Original content from this work may be used under the terms of the [Creative Commons Attribution 3.0 licence](https://creativecommons.org/licenses/by/3.0/). Any further distribution of this work must maintain attribution to the author(s) and the title of the work, journal citation and DOI.

traced back to either purely quantum or classical dynamics [2, 27].

Due to the highly nonlinear nature of ATI, attosecond measurements in the strong-field regime tend to be sensitive to the actual waveform of the electric field and thus require an accurate knowledge of the laser pulse parameters on target, such as pulse duration, carrier-envelope phase (CEP), and peak intensity. So far, however, the accurate determination of the laser intensity on target by measuring the spatial beam properties often remains a challenging and laborious task. An alternative approach to tackle this problem is to use the high sensitivity of ATI to our advantage and utilize the information contained in the photoelectron spectra to determine the laser parameters. The approach of harvesting the information contained in the ATI spectra also allows the measurement of the CEP [28, 29] and pulse duration [30] of few-cycle pulses.

The ATI spectra contain information on the laser intensity: ignoring the interaction of the released electron with the ionic core, a linearly polarized laser field with electric field amplitude E_0 and frequency ω can accelerate the electron to a kinetic energy of up to twice the ponderomotive potential (atomic units are used throughout)

$$U_p = E_0^2 / 4\omega^2. \quad (1)$$

Recollision with the parent ion [9, 31] and subsequent back-scattering enables the electron to reach energies up to $10U_p$ [32]. Although the $2U_p$ or $10U_p$ cut-off energies enable measuring the peak electric field strength, their identification in the spectra is often somewhat ambiguous and yields a relatively large uncertainty of typically 20%. Evaluating the ATI spectra for circular polarization [33] removes some of the ambiguity, as all electrons reach an energy of U_p ⁷. Still, generating perfectly circularly polarized fields is challenging in the few-cycle regime. Recently, a transferable intensity standard based on ionization of atomic hydrogen has been published [34]. However, the method, which consists in the measurement of the intensity-dependent ionization yield from noble gases, requires a separate intensity scan. A similar scheme based on the referencing to hydrogen has also been demonstrated for measuring the absolute CEP [35].

Here, we systematically study the combined intensity and CEP dependence of the longitudinal momentum distribution of ATI of argon over almost one order of magnitude of intensity. We show that the CEP-dependent momentum distribution allows for an unambiguous, precise and accurate intensity determination without the need to perform an intensity scan.

2. Experimental approach

CEP stable few-cycle laser pulses with a duration of 4.5 fs (full width at half maximum of the intensity envelope) and a center wavelength of 750 nm are obtained from a titanium:

⁷ Note that in circularly polarized fields, U_p has twice the value given in equation (1).

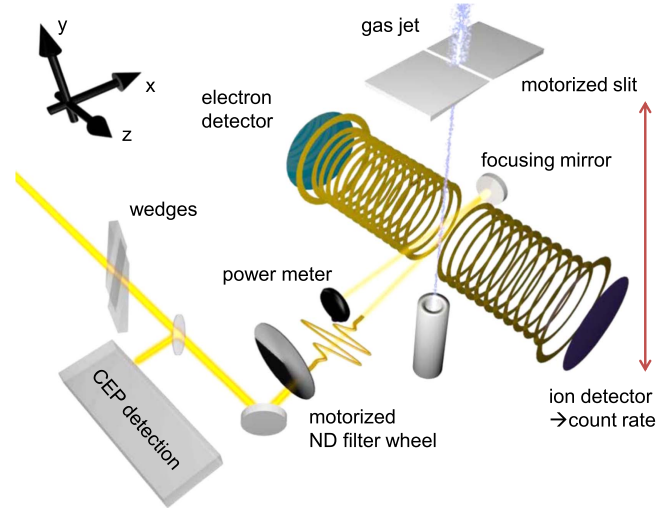


Figure 1. Schematic of the experimental setup. A small fraction of the few-cycle pulses is sent into an f - $2f$ interferometer for CEP detection. The main part passes through a motorized neutral density (ND) filter wheel and is focused ($f = 175$ mm) into a reaction microscope (REMI) where photoelectron and photoion momentum distributions arising from strong-field ionization of argon are recorded. The thickness of the cold gas jet along x can be adjusted using a motorized slit. The arrow on the right side represents a feedback from the ion count rate to the motorized slit, which allows for controlling the count rate over approximately two orders of magnitude. The laser power is recorded with an electronic power meter at the output of the REMI.

sapphire chirped pulse amplifier (Spectra Physics Femtopower HR CEP4) equipped with a gas-filled hollow-core fiber for spectral broadening. After pulse compression using chirped mirrors and fused silica wedges, the beam is sent into the beam path shown in figure 1.

An f - $2f$ interferometer is used to measure the CEP up to a constant offset value. For a quantitative study of the intensity dependence of strong-field ionization, it is important to vary the focal intensity in a well-controlled manner, i.e. without affecting the pulse duration or the focal intensity distribution. To achieve this, we use a neutral density filter wheel (Inconel NiCrFe coating) with an angle dependent transmission. The transmitted pulse energy and, hence, the intensity

$$I = \frac{P}{k}, \quad k = Af_{\text{rep}}\tau = \text{const} \quad (2)$$

is varied by rotating the filter wheel without changing the focal cross section A or pulse duration τ . Here, $f_{\text{rep}} = 9900$ Hz is the laser repetition rate, and P the average laser power, which is recorded with an electronic power meter at the exit of the REMI. In order to avoid false coincidences, the count rate is kept at approximately 0.1–0.15 ions per laser shot by reducing the target thickness when the intensity is increased. This is implemented via a feedback system that controls the width of the motorized slit cutting into the gas jet.

In order to cover a large intensity range, we performed two separate experiments using focal lengths of $f_1 = 17.5$ cm and $f_2 = 10.0$ cm for the low and high intensity regions, respectively.

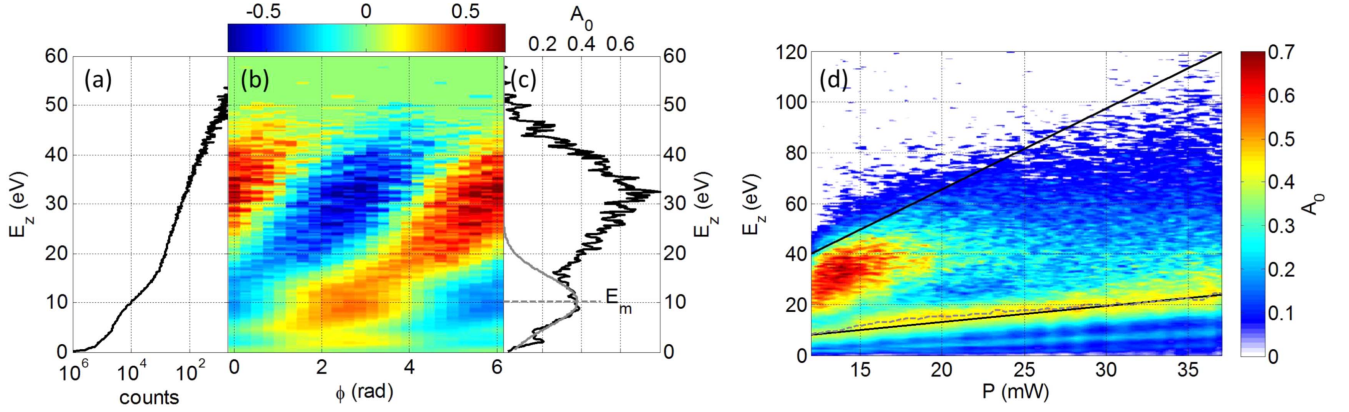


Figure 2. (a) Measured E_z -distribution of Ar^+ ions, where $E_z = p_z^2/2$, and p_z is the momentum component along the laser polarization, for an average laser power of $P = 13.0$ mW. (b) Recorded asymmetry parameter as a function of E_z and CEP. (c) Amplitude $A_0(E_z)$ of the CEP-dependent asymmetry parameter. The position E_m of the local maximum $A_0(E_z)$ near 10 eV is obtained from a Gaussian fit to $A_0(E_z)$ (solid gray line). (d) Measured asymmetry amplitude as a function of E_z and average laser power P . The black solid lines represent estimates for $10 U_p$, and $2 U_p$, respectively. The gray dashed line shows E_m as a function of the average laser power.

3. Results

The experimental results are summarized in figure 2. In panel (a), the number of detected Ar^+ ions recorded at a power $P = (13.0 \pm 0.3)$ mW is plotted as a function of $E_z = p_z^2/2$, where p_z is the ion momentum component along the laser polarization. Note that, due to momentum conservation, the ion momentum has the same magnitude as the photoelectron momentum.

Figure 2(b) shows the CEP-dependent asymmetry in the directional ion yield as a function of E_z and CEP ϕ . The CEP-dependent asymmetry A is defined as

$$A(E_z, \phi) = \frac{N(|p_z|, \phi) - N(-|p_z|, \phi)}{N(|p_z|, \phi) + N(-|p_z|, \phi) + \epsilon}, \quad (3)$$

where $N(|p_z|, \phi)$ and $N(-|p_z|, \phi)$ refer to the number of ions emitted with momentum $|p_z|$ and $-|p_z|$, respectively, and $\epsilon = 1$ is used to avoid division by zero.

For each value of E_z , we extract the amplitude $A_0(E_z)$ of the CEP-dependent asymmetry via Fourier transform of $A(E_z, \phi)$ and analysis of the 2π periodic component. The obtained asymmetry amplitude $A_0(E_z)$, which is plotted in figure 2(c), exhibits several local maxima. Besides the large maximum at energies in the recollision plateau (above 20 eV), two other local maxima are apparent around 10 and 2 eV. The position of the 10 eV maximum, denoted as E_m in the following, is obtained from a Gaussian fit to $A_0(E_z)$ in the region around this peak.

In figure 2(d), the measured E_z -dependent asymmetry amplitude is displayed as a function of the laser power. Notably, the position of the low energy maxima scale linearly with the laser power. The upper black line indicates the position of the high energy ($10 U_p$) cut-off, estimated at low intensity and extrapolated to higher intensity values. The lower black line with a five times smaller slope indicates the estimated position of the $2 U_p$ cut-off. The gray line denotes the positions of the local asymmetry maximum, E_m , obtained

from repeating the procedure outlined above for each recorded laser power. Interestingly, $E_m(P)$ coincides with the black line at $2 U_p$.

To investigate the relationship between E_m and $2 U_p$, we numerically solved the three-dimensional time-dependent Schrödinger equation (3D TDSE) using Qprop [36, 37]. The wavefunction of the initial $3p$ state has been obtained by imaginary time propagation. The effective potential employed in the theoretical description in single-active electron approximation [35, 38] has the form

$$V_{\text{eff}} = -\frac{1}{r} - \frac{Z_{\text{eff}}}{r} \exp(-\alpha r) \quad (4)$$

and ensures the correct long-range $1/r$ -behavior. The effective charge $Z_{\text{eff}} = 12.58$ and the screening length $\alpha = 1.5$ a.u. have been obtained by matching the ionization potential (I_p) to the correct value for argon and by minimizing the deviation of the $3p$ wavefunction from the corresponding prediction of an atomic all-electron Dirac-LDA code. The spectra of the time-dependent calculations are extracted using a window operator method and then analyzed analogously to the experimental data. For the simulation, a laser wavelength of 750 nm, and a pulse duration of 4.5 fs (full width at half maximum of the intensity envelope) are used. The results are averaged over the intensity distribution resulting from a Gaussian beam profile neglecting the variation of the beam waist along the laser propagation, if not otherwise specified.

The measured and calculated intensity dependence of the position of the local asymmetry maximum E_m are compared in figure 3. For the calibration of the experimental intensity, only the proportionality constant between focal intensity and recorded laser power needs to be adjusted (see equation (2)). We find $k_1 = 0.1558$ mW $(\text{TW cm}^{-2})^{-1}$ for experiment 1 and $k_2 = 0.0424$ mW $(\text{TW cm}^{-2})^{-1}$ for experiment 2. Over the entire range of the two measurements, $E_m(I)$ remains close to the $2 U_p$ line. As shown in the inset, the deviation is always smaller than 20% and for most intensities smaller than 10%.

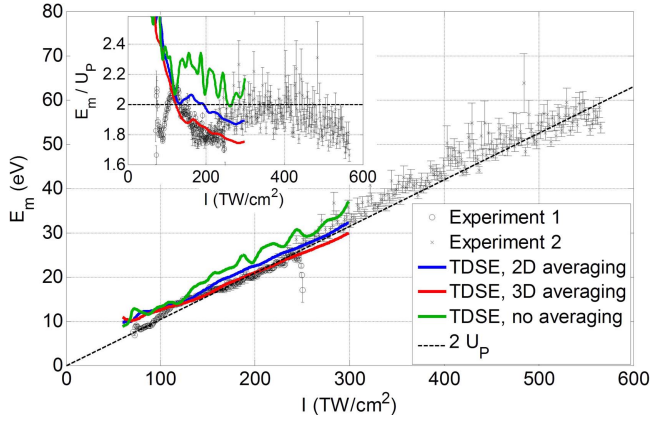


Figure 3. Measured and calculated intensity dependence of the position E_m of the asymmetry maximum. Shown are the results of two separate experiments, covering different intensity ranges. Theoretical results are shown for focal volume averaging with constant beam waist (2D), and varying beam waist (3D), and without focal volume averaging. The dashed black line indicates $2 U_p$. The inset shows E_m in units of U_p .

4. Discussion

For intensities above $9 \times 10^{13} \text{ W cm}^{-2}$, the theoretical results confirm the empirical observation that E_m is associated with the direct electron cut-off at $2 U_p$. Thus, the measurement of E_m yields an estimate for the peak intensity given by:

$$I \approx (E_m / 12 \text{ eV})(\lambda / 800 \text{ nm}) 10^{14} \text{ W cm}^{-2}. \quad (5)$$

The precision of the experimental intensity determination decreases for high intensities where the asymmetry maximum at E_m becomes broader. The data presented in figure 3 contains approximately 1 million counts for each intensity value, more than 400 million counts in total, acquired over a period of 120 h.

To test the robustness of the intensity calibration with respect to the focal intensity distribution, we average the calculated spectra over the focal volume for two different scenarios. In the first scenario, the signal is averaged over the focal plane (i.e. over two dimensions), thus neglecting the variation of the beam waist along the laser propagation direction. This represents a good approximation when the extension of the gas target along the laser propagation direction is much smaller than the Rayleigh range. In the second scenario, we take the variation of the beam waist along the laser propagation into account, and integrate over the full 3D intensity distribution in the focus of a Gaussian beam. This represents a good approximation when the extension of the gas target along the laser propagation direction is larger than the Rayleigh range. The results of these two calculations are compared to those obtained at the peak intensity only. As can be seen in figure 3, the intensity averaging has two effects. First, it washes out modulations visible in the fixed-intensity results (green line). Second, it reduces the effective intensity of the laser focus, as intensities lower than the peak value contribute to the intensity-averaged yield. In the 3D case, the contribution of lower intensities is larger than in the 2D case, resulting in a lower effective intensity. The difference between 2D and 3D averaging amounts to approximately 10% and can be considered a good measure for typical uncertainties

of the focal shape. The transition from 2D to 3D focal volume averaging as the size of the gas jet is increased with respect to the size of the laser focus has been discussed in detail in [39].

At intensities below 100 TW cm^{-2} , the TDSE results deviate from the experimental results. We attribute these deviations to inaccuracies of the short-range behavior of the effective potential used for the TDSE. The deviations also suggest that slow electrons may be particularly sensitive to the effective potential landscape, which is, in turn, particularly hard to model close to the ionic core, where electron correlations play a more important role.

The accurate determination of the experimental intensity on target facilitates the detailed discussion of the combined intensity and CEP dependence of the photoelectron spectra. To this end, we plot in figure 4 the measured and predicted asymmetry amplitudes as a function of intensity and E_z , in units of U_p .

We first discuss the behavior of the region of rescattered electrons, $E > 4 U_p$. As can be seen in figures 4(a) and (b), the high energy cut-off decreases with increasing intensity. In the TDSE results, this decrease is rather consistent with the formula for the cut-off energy $E_c = 10 U_p + 0.538 I_p$ given in [40], which is represented by the dashed black line. We attribute the faster decrease of the asymmetry amplitude in the experimental data to the limited signal-to-noise ratio. As shown in figure 4(d), the ratio of recollision and direct electrons signal indeed decreases with increasing intensity, which can be understood as a consequence of the decreasing rescattering probability with increasing electron energy. Another prominent feature in figures 4(a) and (b) is the decrease of the asymmetry amplitude in the rescattering region at higher intensity. This may be due to the onset of saturation of the ionization probability, which washes out the contrast of ionization probability for half-cycles with slightly different field strengths.

We now turn towards the region of direct electrons $E \leq 2 U_p$. The most prominent feature is the large horizontal bar at $2 U_p$. We further observe two additional local asymmetry maxima, as indicated by the arrows in figure 4(c). The maximum at $0.8 U_p$ corresponds to the maximum observed in figure 2(c) at 2 eV. The maximum at $0.3 U_p$ emerges only at intensities above 120 TW cm^{-2} in the experimental data (see figure 5(a)). The observed maxima are attributed to intracycle interferences [41–43]. These interferences result from the fact that there are two quantum trajectories of direct electrons ionized at two different instants within the same laser cycle, which lead to the same final momentum state. The intracycle interference structures, which were initially observed in above threshold detachment spectra of negative ions [44, 45], were shown to govern the shape of the photoelectron spectra [23]. In the context of strong-field ionization of atoms with few-cycle pulses, the intracycle interference effect leads to CEP-dependent modulations of the ATI spectra [24].

In order to support the claim that the observed maxima result from intracycle interferences, we have performed a 1D semi-classical simulation of interferences in the ATI spectra produced by 4.5 fs, 750 nm laser pulses of different intensities. For a given final momentum p , electron trajectories are launched at all points in time t_n satisfying $A(t_n) = p$. The phase of each trajectory is calculated by computing the action

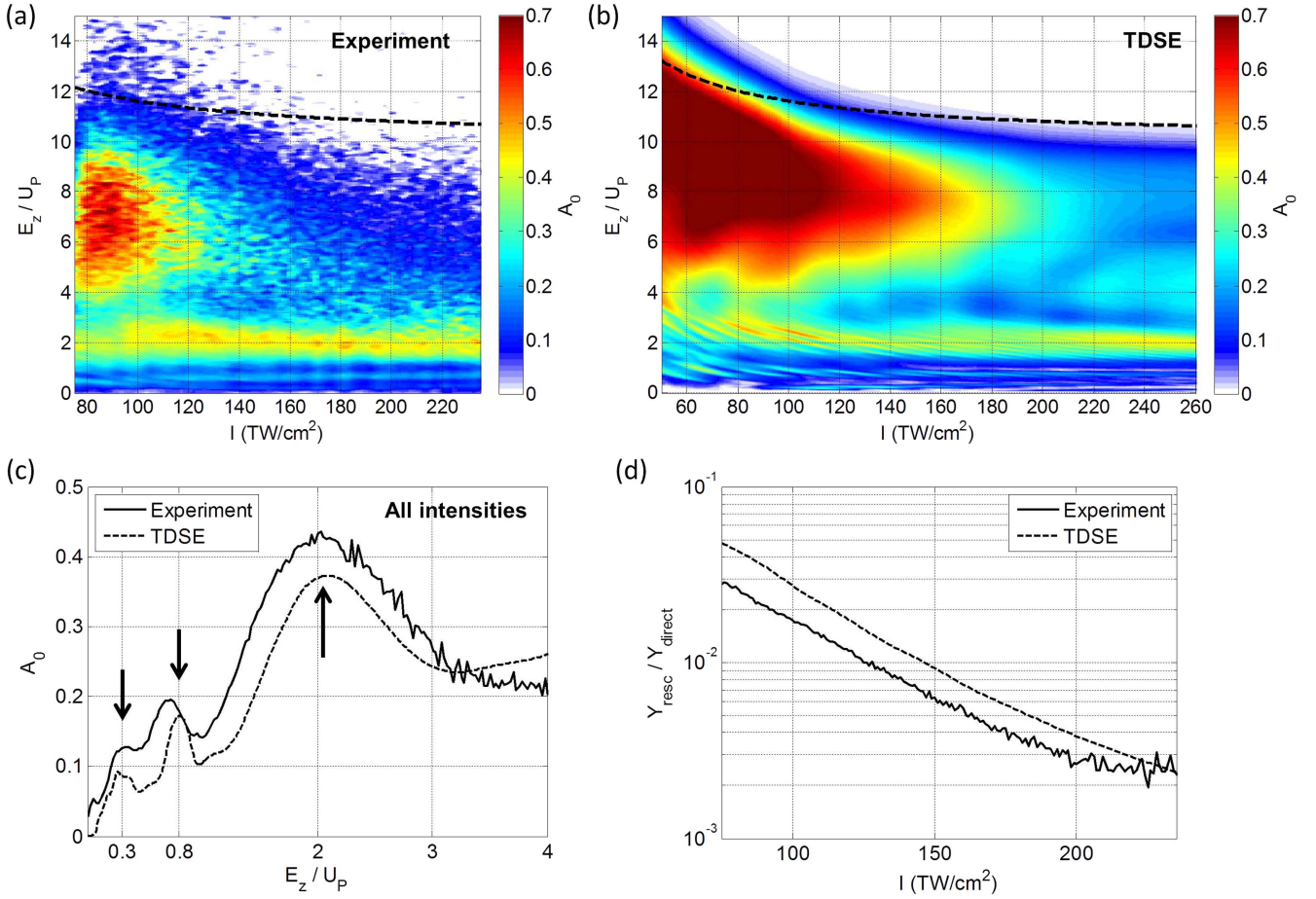


Figure 4. Measured (a) and calculated (b) asymmetry amplitude as a function of E_z and intensity, where E_z is expressed in units of U_p . The black dashed line represents the cut-off law given in [40]. (c) Asymmetry amplitude as a function of E_z in units of U_p , integrated over all intensities. The position of the local maxima of the asymmetry amplitude below $2U_p$ are marked with arrows. (d) Calculated and measured ratio of the yields for rescattered (with $4U_p < E_z < 10U_p$) and direct electrons (with $0.5U_p < E_z < 2U_p$).

S of a trajectory as follows

$$S(t_n) = S_g(t_n) + S_a(t_n) + S_c(t_n), \quad (6)$$

$$S_g(t_n) = \int_0^{t_n} -I_p dt, \quad (7)$$

$$S_a(t_n) = \text{sgn}[-E(t_n)] \pi/2, \quad (8)$$

$$S_c(t_n) = \int_{t_n}^{\infty} [A(t) - A(t_n)]^2 / 2 dt. \quad (9)$$

The atomic action S_a takes into account the parity of the groundstate p orbital.

The ionization probability for each trajectory $R(t_n)$ is calculated using the ionization rates given in [46]. The photoelectron spectrum is calculated as

$$W(p) = \left| \sum_n \sqrt{R(t_n)} \exp(iS(t_n)) \right|^2. \quad (10)$$

The CEP-dependent asymmetry is obtained from the spectra following the same procedure as for the TDSE results. We present in figure 5 the measured and calculated asymmetry amplitude maps in the range below $2U_p$.

The asymmetry maxima highlighted in figure 4(c) are clearly visible and marked by arrows in the experimental and TDSE results shown in figures 5(a) and (b), respectively. A qualitatively similar series of nearly horizontal maxima can be

seen in the results of the semi-classical calculations shown in figure 5(c), while it is absent in figure 5(d). There, intracycle interferences are artificially switched off by considering only one of the two interfering trajectories within each cycle, but allowing *intercycle* interferences. This indicates that the intracycle interference effect is indeed responsible for the observed horizontal series of asymmetry maxima.

In addition to the intracycle interferences, the TDSE results exhibit strong periodic and intensity-dependent modulations that are most pronounced at low intensities. The comparison to the curved dashed lines in figure 5 shows that the periodic maxima in the asymmetry amplitude can be associated with a series ($n = 10, 11, 12, \dots$) of ponderomotively shifted ATI peaks, arising from *intercycle* interferences, given by

$$E_n/U_p = (n\hbar\omega - I_p)/U_p - 1. \quad (11)$$

The spacing of the ATI maxima are consistent with modulations visible in the experimental data (figure 5(a)) and semi-classical results (figures 5(c) and (d)).

We observe that the amplitude of the asymmetry is modulated by both, ATI peaks [47] and intracycle interferences [48]. Further investigations are needed to determine the reasons for the residual mismatch between TDSE results and experiment. As pointed out above, inaccuracies in the model potential

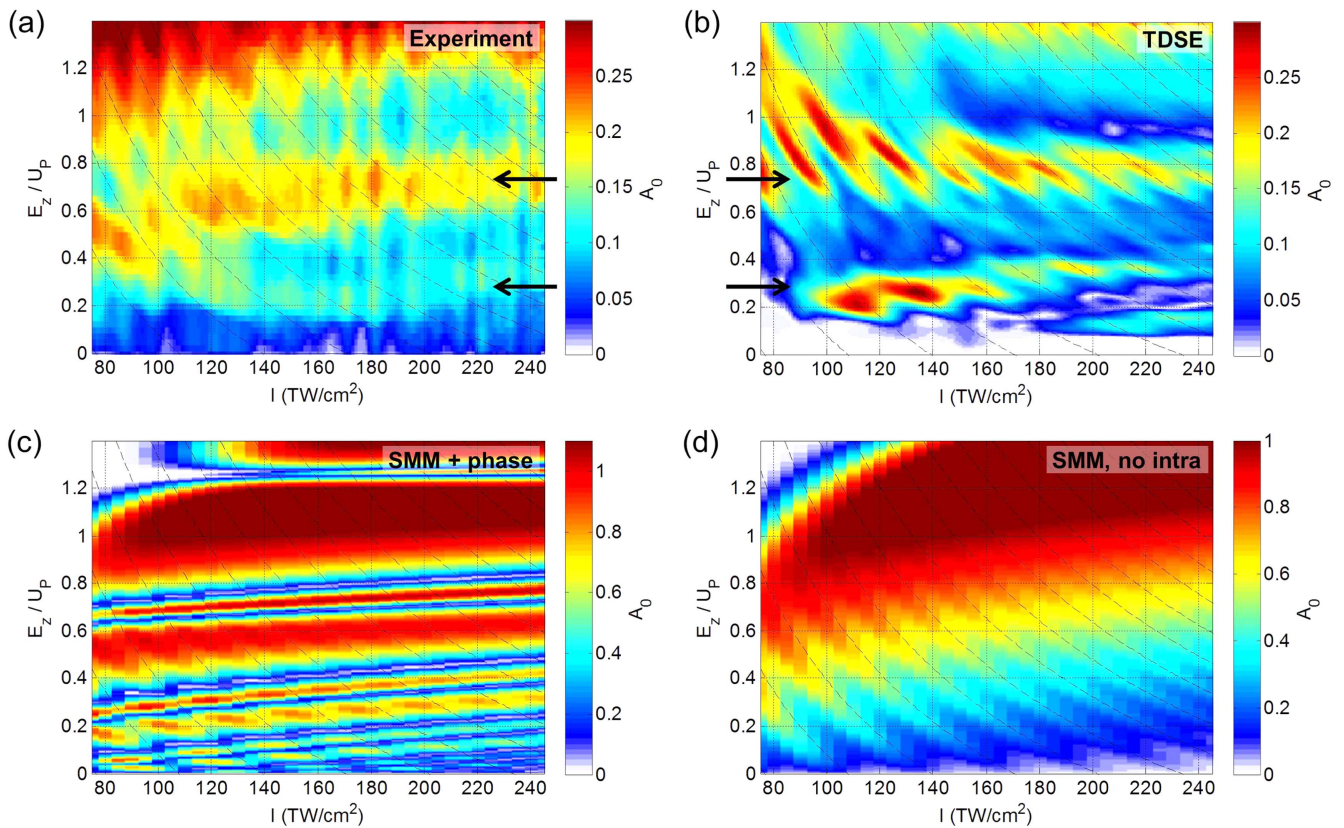


Figure 5. Close up view of the measured (a) and simulated (b)–(d) asymmetry amplitude at low energies. The arrows mark the position of the features highlighted in figure 4(c). The dashed lines mark the expected peak positions of an ATI comb with a spacing corresponding to the laser wavelength of 750 nm, taking the ponderomotive shift of the peaks into account. Panel (b) shows results of the 3D TDSE. Panel (c) shows results for the extended simple man’s model (SMM) with interferences. In panel (d), intracycle interferences are artificially switched off.

used for argon in the 3D TDSE simulations most likely affect low energy electrons. The observed features reflect the structure of the ionic potential. Thus, in principle, they could be used to benchmark model potentials for atomic or molecular targets.

5. Conclusion

In conclusion, our systematic study of ATI of argon as a function of CEP and intensity in the few-cycle regime has revealed that the direct electron cut-off at $2 U_p$ is characterized by a pronounced maximum of the CEP-dependent asymmetry. This feature provides a convenient benchmark for a robust and accurate peak intensity determination of linearly polarized few-cycle pulses over a large intensity range, and without the need for performing a separate intensity scan. The rich structure observed in the CEP-dependent asymmetry amplitude of ATI results from an interplay of ponderomotively shifted ATI peaks and intracycle interference.

Acknowledgments

We acknowledge fruitful discussions with D Bauer and T Pfeifer. MK, MFK, and BB acknowledge support from the Max Planck Society and the DFG via SPP1840,

LMUexcellent, and the cluster of excellence ‘Munich Centre for Advanced Photonics’ (MAP). We are grateful for support by the European Union via the ERC project ATTOCO (307203) and the H2020 project ATTOCHEM (657544). TF acknowledges support from the DFG via SFB652, SPP1840, and a Heisenberg fellowship. Computer time has been provided by the North German Supercomputing Alliance (HLRN) within project mvp00010.

ORCID iDs

M Kübel <https://orcid.org/0000-0001-6065-6122>
 T Fennel <https://orcid.org/0000-0002-4149-5164>
 M F Kling <https://orcid.org/0000-0002-1710-0775>

References

- [1] Agostini P, Fabre F, Mainfray G, Petite G and Rahman N 1979 Free-free transitions following six-photon ionization of xenon atoms *Phys. Rev. Lett.* **42** 1127–30
- [2] Becker W, Grasbon F, Kopold R, Milošević D B, Paulus G G and Walther H 2002 Above-threshold-ionization: from classical features to quantum effects *Adv. At. Mol. Opt. Phys.* **48** 35–98

- [3] Milošević D B, Paulus G G, Bauer D and Becker W 2006 Above-threshold ionization by few-cycle pulses *J. Phys. B: At. Mol. Opt. Phys.* **39** R203–62
- [4] Ferray M, L'Huillier A, Fi X F, Lompre L A, Mainfray G and Manus C 1988 Multiple-harmonic conversion of 1064 nm radiation in rare gases *J. Phys. B: At. Mol. Opt. Phys.* **21** L31
- [5] Hentschel M, Kienberger R, Spielmann Ch, Reider G A, Milosevic N, Brabec T, Corkum P B, Heinzmann U, Drescher M and Krausz F 2001 Attosecond metrology *Nature* **414** 509–13
- [6] Krausz F and Ivanov M 2009 Attosecond physics *Rev. Mod. Phys.* **81** 163–234
- [7] Freeman R R, Bucksbaum P H, Milchberg H, Darack S, Schumacher D and Geusic M E 1987 Above-threshold ionization with subpicosecond laser pulses *Phys. Rev. Lett.* **59** 1092–5
- [8] Corkum P B, Burnett N H and Brunel F 1989 Above-threshold ionization in the long-wavelength limit *Phys. Rev. Lett.* **62** 1259–62
- [9] Schafer K J, Yang B, DiMauro L F and Kulander K C 1993 Above threshold ionization beyond the high harmonic cutoff *Phys. Rev. Lett.* **70** 1599–602
- [10] Paulus G G, Nicklich W, Xu H L, Lambropoulos P and Walther H 1994 Plateau in above-threshold ionization spectra *Phys. Rev. Lett.* **72** 2851–4
- [11] Grasbon F, Paulus G, Walther H, Villaresi P, Sansone G, Stagira S, Nisoli M and De Silvestri S 2003 Above-threshold ionization at the few-cycle limit *Phys. Rev. Lett.* **91** 173003
- [12] Kling M F, Rauschenberger J, Verhoef A J, Hasović E, Uphues T, Milošević D B, Müller H G and Vrakking M J J 2008 Imaging of carrier-envelope phase effects in above-threshold ionization with intense few-cycle laser fields *New J. Phys.* **10** 025024
- [13] Blaga C I, Catoire F, Colosimo P, Paulus G G, Müller H G, Agostini P and DiMauro L F 2009 Strong-field photoionization revisited *Nat. Phys.* **5** 335–8
- [14] Bergues B, Zherebtsov S, Deng Y, Gu X, Znakovskaya I, Kienberger R, Krausz F, Marcus G and Kling M F 2011 Sub-cycle electron control in the photoionization of xenon using a few-cycle laser pulse in the mid-infrared *New J. Phys.* **13** 063010
- [15] Eckle P, Pfeiffer A N, Cirelli C, Staudte A, Dörner R, Müller H G, Büttiker M and Keller U 2008 Attosecond ionization and tunneling delay time measurements in helium *Science* **322** 1525–9
- [16] Pfeiffer A N, Cirelli C, Smolarski M, Dörner R and Keller U 2011 Timing the release in sequential double ionization *Nat. Phys.* **7** 428–33
- [17] Meckel M *et al* 2008 Laser-induced electron tunneling and diffraction *Science* **320** 1478–82
- [18] Blaga C I, Xu J, Dichiaro A D, Sistrunk E, Zhang K, Agostini P, Miller T A, DiMauro L F and Lin C D 2012 Imaging ultrafast molecular dynamics with laser-induced electron diffraction *Nature* **483** 194–7
- [19] Boguslavskiy A E, Mikosch J, Gijbertsen A, Spanner M, Patchkovskii S, Gador N, Vrakking M J J and Stolow A 2012 The multielectron ionization dynamics underlying attosecond strong-field spectroscopies *Science* **335** 1336–40
- [20] Skruszewicz S, Tiggesbäumker J, Meiwes-Broer K-H, Arbeiter M, Fennel T and Bauer D 2015 Two-color strong-field photoelectron spectroscopy and the phase of the phase *Phys. Rev. Lett.* **115** 043001
- [21] Wolter B *et al* 2016 Ultrafast electron diffraction imaging of bond breaking in di-ionized acetylene *Science* **354** 308–12
- [22] Paulus G G, Grasbon F, Walther H, Kopold R and Becker W 2001 Channel-closing-induced resonances in the above-threshold ionization plateau *Phys. Rev. A* **64** 021401
- [23] Bergues B, Ansari Z, Hanstorp D and Kiyan I Y 2007 Photodetachment in a strong laser field: an experimental test of Keldysh-like theories *Phys. Rev. A* **75** 063415
- [24] Gopal R *et al* 2009 Three-dimensional momentum imaging of electron wave packet interference in few-cycle laser pulses *Phys. Rev. Lett.* **103** 053001
- [25] Wu C Y, Yang Y D, Liu Y Q and Gong Q H 2012 Characteristic spectrum of very low-energy photoelectron from above-threshold ionization in the tunneling regime *Phys. Rev. Lett.* **109** 043001
- [26] Wolter B, Pullen M G, Baudisch M, Sclafani M, Hemmer M, Senftleben A, Schröter C D, Ullrich J, Moshhammer R and Biegert J 2015 Strong-field physics with mid-IR fields *Phys. Rev. X* **5** 021034
- [27] Popruzhenko S V 2014 Keldysh theory of strong field ionization: history, applications, difficulties and perspectives *J. Phys. B: At. Mol. Opt. Phys.* **47** 204001
- [28] Paulus G G, Lindner F, Walther H, Baltuska A, Goulielmakis E, Lezius M and Krausz F 2003 Measurement of the phase of few-cycle laser pulses *Phys. Rev. Lett.* **91** 253004
- [29] Rathje T, Johnson N G, Möller M, Süßmann F, Adolph D, Kübel M, Kienberger R, Kling M F, Paulus G G and Saylor A M 2012 Review of attosecond resolved measurement and control via carrier-envelope phase tagging with above-threshold ionization *J. Phys. B: At. Mol. Opt. Phys.* **45** 074003
- [30] Saylor A M, Rathje T, Müller W, Kürbis C, Rühle K, Stibenz G and Paulus G G 2011 Real-time pulse length measurement of few-cycle laser pulses using above-threshold ionization *Opt. Express* **19** 4464–71
- [31] Corkum P B 1993 Plasma perspective on strong-field multiphoton ionization *Phys. Rev. Lett.* **71** 1994–7
- [32] Paulus G G, Becker W, Nicklich W and Walther H 1994 Rescattering effects in above-threshold ionization: a classical model *J. Phys. B: At. Mol. Opt. Phys.* **27** L703–8
- [33] Alnaser A S, Tong X M, Osipov T, Voss S, Maharjan C M, Shan B, Chang Z and Cocke C L 2004 Laser-peak-intensity calibration using recoil-ion momentum imaging *Phys. Rev. A* **70** 1–6
- [34] Wallace W C *et al* 2016 Precise and accurate measurements of strong-field photoionization and a transferable laser intensity calibration standard *Phys. Rev. Lett.* **117** 1–5
- [35] Saylor A M *et al* 2015 Accurate determination of absolute carrier-envelope phase dependence using photo-ionization *Opt. Lett.* **40** 3137–40
- [36] Bauer D and Koval P 2006 Qprop: a Schrödinger-solver for intense laseratom interaction *Comput. Phys. Commun.* **174** 396–421
- [37] Mosert V and Bauer D 2016 Photoelectron spectra with qprop and t-surff *Comput. Phys. Commun.* **207** 452–63
- [38] Müller H G 1999 Numerical simulation of high-order above-threshold-ionization enhancement in argon *Phys. Rev. A* **60** 1341–50
- [39] Kübel M *et al* 2016 Complete characterization of single-cycle double ionization of argon from the nonsequential to the sequential ionization regime *Phys. Rev. A* **93** 053422
- [40] Busuladzic M, Gazibegovic-Busuladzic A and Milosevic D B 2006 High-order above-threshold ionization in a laser field: influence of the ionization potential on the high-energy cutoff *Laser Phys.* **16** 289–93
- [41] Gribakin G F and Kuchiev M Y 1997 Multiphoton detachment of electrons from negative ions *Phys. Rev. A* **55** 3760–71
- [42] Kopold R and Becker W 1999 Interference in high-order above-threshold ionization *J. Phys. B: At. Mol. Opt. Phys.* **32** L419
- [43] Kopold R, Becker W and Kleber M 2000 Quantum path analysis of high-order above-threshold ionization *Opt. Commun.* **179** 39–50

- [44] Reichle R, Helm H and Kiyani I Y 2001 Photodetachment of H- in a strong infrared laser field *Phys. Rev. Lett.* **87** 243001
- [45] Reichle R, Helm H and Kiyani I Y 2003 Detailed comparison of theory and experiment of strong-field photodetachment of the negative hydrogen ion *Phys. Rev. A* **68** 063404
- [46] Tong X M and Lin C D 2005 Empirical formula for static field ionization rates of atoms and molecules by lasers in the barrier-suppression regime *J. Phys. B: At. Mol. Opt. Phys.* **38** 2593–600
- [47] Abel M J, Pfeifer T, Jullien A, Nagel P M, Bell M J, Neumark D M and Leone S R 2009 Carrier-envelope phase-dependent quantum interferences in multiphoton ionization *J. Phys. B: At. Mol. Opt. Phys.* **42** 075601
- [48] Arbó D G, Ishikawa K L, Schiessl K, Persson E and Burgdörfer J 2010 Intracycle and intercycle interferences in above-threshold ionization: the time grating *Phys. Rev. A* **81** 021403